Molecular Therapy
Oncology
Original Article

Use of patient-derived organotypic tumor spheroids for testing of viral vector gene therapy in combination with checkpoint blockade

Ana Carolina M. Domingues,[1,2] Soraia B. de Oliveira,[1] Nayara G. Tessarollo,[1,6] Ana Paula Lepique,[1,3] Otavio Rodrigues,[1] Tatyana Sharova,[2] Aleigha Lawless,[2] David Li,[2] Madak Basnet,[2] Genevieve M. Boland,[4,5] Sonia Cohen,[4] Russell W. Jenkins,[2,5] and Bryan E. Strauss[1]

[1]Instituto do Câncer do Estado de São Paulo, Hospital das Clínicas, Faculdade de Medicina, Universidade de São Paulo, São Paulo 01246-000, Brazil; [2]Mass General Cancer Center, Krantz Family Center for Cancer Research, Department of Medicine, Massachusetts General Hospital, Harvard Medical School, Boston, MA 02114, USA; [3]Department of Immunology, Universidade de São Paulo, São Paulo 05508-000, Brazil; [4]Division of Gastrointestinal and Oncologic Surgery, Department of Surgery, Massachusetts General Hospital, Harvard Medical School, Boston, MA 02114, USA; [5]Broad Institute of MIT and Harvard, Cambridge, MA 02142, USA

Checkpoint inhibitors have revolutionized cancer treatment, but a significant proportion of patients do not respond to these therapies, underscoring the need for alternative strategies. Although gene therapy has made substantial strides, its application in solid tumors remains underexplored, with limited treatments approved. Here, we further investigated a gene therapy approach with non-replicating adenoviral vectors encoding the alternate reading frame (ARF) and interferon beta (IFNb) and tested it in a clinically relevant setting. We previously showed that this combined gene therapy induces immunogenic cell death in melanoma models, and now, we utilize patient-derived organotypic tumor spheroids (PDOTS), a model that closely recapitulates the immune environment of tumors, to test its effects using patient tumors. Our results demonstrate, for the first time, the effectiveness of using PDOTS to evaluate viral-vector-based gene therapies. While the addition of anti-PD-1 did not enhance therapeutic outcomes, the gene therapy alone suppressed tumor growth and triggered antitumor immune responses across different cancer models, notably those with low immunogenicity and specific genome profiles. These findings suggest that this gene therapy could serve as a valuable alternative for patients not responsive to checkpoint inhibitors and who have solid tumors with limited treatment and impaired p53-ARF-MDM2 pathways, such as liposarcomas.

INTRODUCTION

The advent of checkpoint inhibitors transformed cancer therapy, yet the proportion of patients unresponsive or refractory to these agents remains alarming.[1] Therefore, new therapeutic alternatives are needed for patients for whom checkpoint inhibitors are ineffective. Within more recent years, gene therapy re-emerged with the potential to once again reshape the field of oncology, particularly with the success of chimeric antigen receptor (CAR)-T cells in treating hematologic malignancies.[2] However, although solid tumors account for the majority of cancer cases, there are still few approved gene therapies available for these tumors, leaving many patients with limited therapeutic options.[3,4]

Building on this unmet need, we previously demonstrated that a combined gene therapy approach using non-replicating adenoviral vectors encoding the alternate reading frame (ARF) and interferon beta (IFNb) promotes immunogenic cell death across various mouse and human melanoma models.[5–7] While ARF is expected to promote cell death by liberating p53 from MDM2, we and others have shown an increasingly important role for the p53 pathway in promoting antitumor immune signals.[8,9] IFNb, well known for its immune-activating properties, also promotes cell death that is aided by the p53/ARF pathway.[10,11]

To further explore its potential, we sought to evaluate this candidate gene therapy in a clinically relevant model that closely mimics the tumor immune microenvironment. Although patient-derived organotypic tumor spheroids (PDOTS) have been utilized to assess CAR-T cell therapy therapeutic effects,[12,13] our study is the first to successfully employ PDOTS to evaluate the efficacy of viral-vector-based gene therapies.

RESULTS

PDOTS is a feasible platform for testing viral-vector-based gene therapies

To test our gene therapy approach in a clinically relevant model that recapitulates the tumor immune context, we used PDOTS. To explore

Received 23 October 2024; accepted 24 January 2025;
https://doi.org/10.1016/j.omton.2025.200942.

[6]Present address: Instituto Nacional de Câncer (INCA), Rio de Janeiro 20230-130, Brazil

Correspondence: Bryan E. Strauss, Instituto do Câncer do Estado de São Paulo, Hospital das Clínicas, Faculdade de Medicina, Universidade de São Paulo, São Paulo 01246-000, Brazil.
E-mail: bstrauss@usp.br

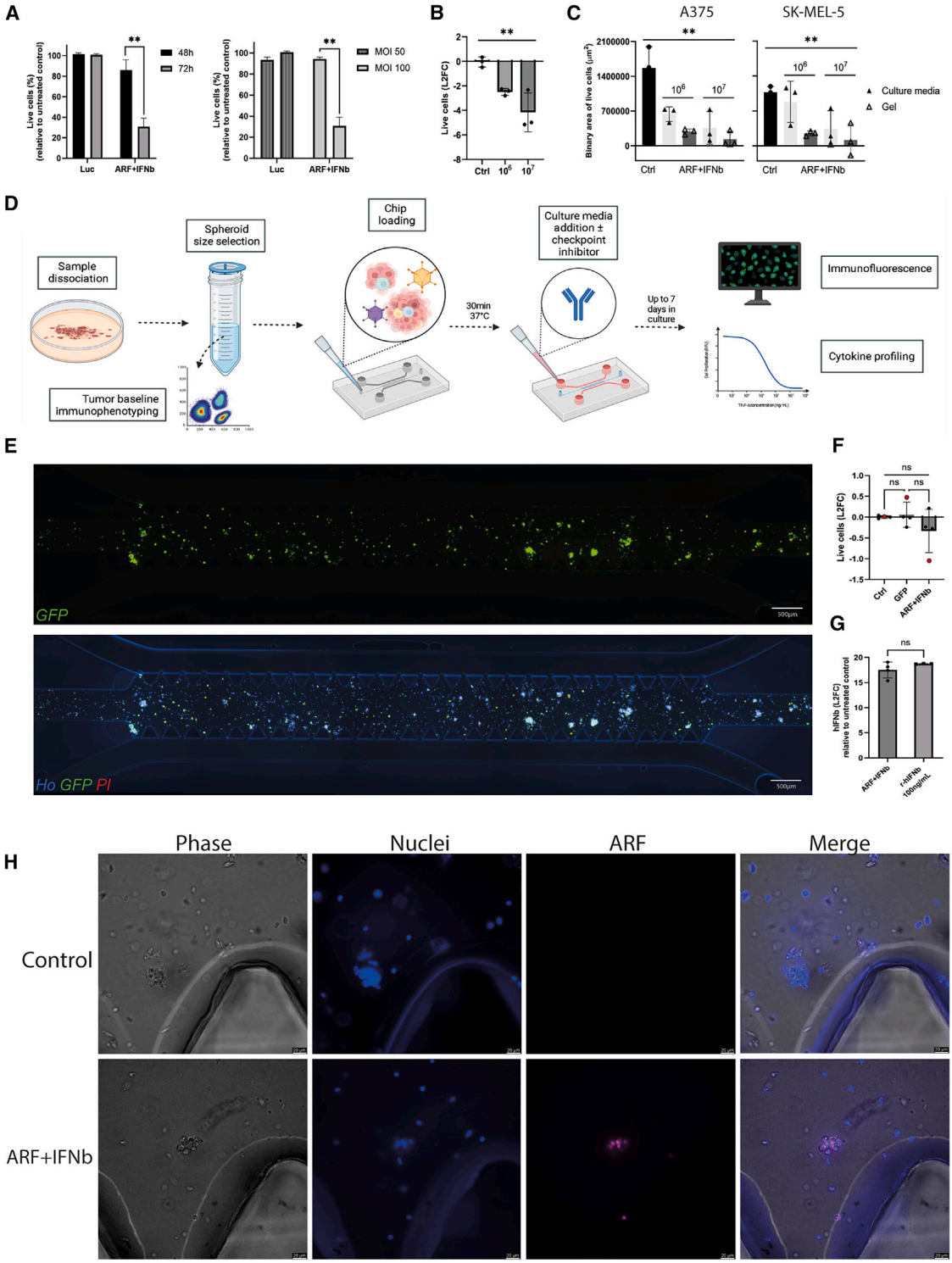

Figure 1. Establishment of on-chip gene therapy with adenoviral vectors using PDOTS

(A) Viability of A375 cells ($n = 3$) in monolayer 48 or 72 h post-treatment with ARF+IFNb at a multiplicity of infection (MOI) of 100 for each vector, assessed by flow cytometry. (B) Viability of monotypic tumor spheroids (MTS) obtained from A375 cells ($n = 3$) after 72 h of on-chip treatment with 2×10^6 or 10^7 total transducing units (TU) of ARF+IFNb assessed by fluorescence microscopy and expressed as log2 fold change (L2FC) of ARF+IFNb or Luc relative to untreated control. (C) Viability of MTS obtained from A375 or

(legend continued on next page)

the feasibility of this assay, firstly, A375 human melanoma cells were transduced with the vectors using the conventional two-dimensional (2D) model, and a time- and dose-dependent response was observed (Figure 1A). Then, the A375 cells were used to generate monotypic tumor spheroids (MTS) and were loaded on a chip. As the results with the same cell line in the 3D model were comparable to those in the 2D model (Figure 1B), we continued to evaluate the best route of vector administration for the gene therapy on a chip. We treated MTS from two cell lines by adding the virus to the collagen mix before loading the chip and adding it to the culture media. Since the results in Figure 1C showed superior control of tumor growth when the viral vectors were added to the collagen mix and this also closely mimics the *in situ* administration of vectors for *in vivo* models, we decided to proceed by adding the virus to the collagen-spheroid mix before loading the chip. With the protocol established, the PDOTS were prepared, loaded in microfluidic devices in collagen hydrogels mixed with the viral vectors, and incubated for up to 7 days (Figure 1D). Melanoma PDOTS treated with the control vector encoding GFP were efficiently transduced (Figure 1E) with no disturbance of cell viability (Figure 1F). Out of the four random PDOTS transduced in parallel with the control (GFP) and therapeutic vectors (ARF+IFNb), only one responded to the gene therapy (red dots), and yet no decrease in cell viability was observed using the control vector (Figure 1F). A week after the treatment with ARF+IFNb, IFNb levels in the conditioned media of PDOTS were equivalent to 100 ng/mL of recombinant human IFNb (Figure 1G), and nuclear expression of ARF was detected in the treated group only (Figure 1H). These data show that PDOTS can be successfully transduced on a chip by adenoviral vectors and promote efficient transgene expression.

ARF+IFNb gene therapy controls tumor progression of cold and immune-exhausted tumors in a clinically relevant model

Once the platform for testing the gene therapy was established, PDOTS were prepared from explanted patient tumors (n = 19) and treated with ARF+IFNb gene therapy. Over half the PDOTS (53%, p = 0.0377) responded to the gene therapy, with responders being well distributed between different histology types (Figure 2A). The analysis of the conditioned media of PDOTS treated with the gene therapy relative to the untreated control showed that cytokine overexpression was primarily present in responders, and, inversely, most downregulated/unaltered cytokines were seen in unresponsive PDOTS (Figure 2B). Nonetheless, the major change in cytokine expression was an increase in IP-10 levels across responders (Figure 2B). From the responder group, 60% were primary tumors (6/10) with either low or high tumor mutational burden (TMB) (Figure 2C). A baseline immunophenotyping of the untreated specimens used for PDOTS showed that all tumors with low immune cell infiltration, except for melanomas, responded to ARF+IFNb (Figures 2D and S1). In addition, the PDOTS response did not correlate to the baseline expression of exhaustion markers on infiltrated CD8 T cells, showing that the gene therapy can control the growth of immune-exhausted tumors (Figure 2E). To analyze whether the vector could transduce the infiltrated immune cells, a human melanoma cell line established by our group was co-cultured with autologous TILs (tumor-infiltrated CD8+ lymphocytes) and treated with the GFP vector. No green fluorescence was detected on TILs after 5 days of treatment (Figures 2F and 2G). As the gene therapy aims to reestablish the p53 pathway of tumors with the functional but impaired protein, we evaluated the response of PDOTS to the gene therapy under a p53-responsive promoter (PGTxb [PG]). The p53 in the transduced cells binds to the PG site and promotes ARF expression, which initiates a positive feedback loop, in which the expression of ARF releases p53 from MDM2 degradation and, in turn, increases transgene expression (Figure 2H). To test the response of PDOTS to the combined gene therapy with the p53-responsive promoter (PG), eight PDOTS from the main cohort (n = 19; Figure 2A) were treated in parallel to a-PD-1 and ARF+IFNb (cytomegalovirus [CMV]) with ARF+IFNb (PG). Not only did the response increase from 38% with the constitutive promoter (CMV) to 50% with the p53-responsive promoter (PG), but it was observed in three melanomas with wild-type (WT) TP53 and deleted/mutated CDKN2A (which encodes ARF) that had not responded to ARF+IFNb (CMV). This shows that the gene therapy under the PG promoter can benefit patients with specific subsets of tumors and that CDKN2A status predicts the response to ARF+IFNb (PG) but not ARF+IFNb (CMV) (Figure 2I). Lastly, IFNb levels detected in the conditioned media of PDOTS treated with ARF+IFNb (PG) were higher than the expression in PDOTS treated with the same dose of ARF+IFNb (CMV). These findings demonstrate that the ARF+IFNb gene therapy can benefit a set of patients who are not responsive to other immunotherapy strategies and that the PG promoter is superior for tumors with WT *TP53* but altered *CDKN2A*.

PD-(L)1 is upregulated upon gene transfer of ARF+IFNb, but combination with checkpoint inhibitors is not superior to the gene therapy alone

It has been shown that functional p53 and type 1 IFN pathways induce PD-L1 expression.[14,15] Therefore, we tested whether ARF+IFNb-treated mouse melanoma cells would upregulate PD-L1. We observed that not only did the gene therapy upregulate the surface expression of this protein, but this increase was directly proportional to transgene expression, as shown by GFP expression correlating to PD-L1 upregulation over time on treated cells (Figures 3A–3C). These results indicate that ARF+IFN are responsible for this

SK-MEL-5 cell lines treated for 5 days with 10^6 or 10^7 total TU of ARF+IFNb administered via collagen-spheroid mix or culture media. (D) Schematic representation of sequential steps for PDOTS establishment and treatment. (E) Fluorescence images of melanoma PDOTS transduced with 2×10^7 total TU of GFP vector (green) and stained for nuclei with Hoechst (blue) and dead cells with PI (red). (F) Viability of PDOTS (n = 4) upon treatment with 2×10^7 total TU of control (GFP) or therapeutic vectors (ARF+IFNb) expressed as L2FC of ARF+IFNb or GFP relative to untreated control. The responder (to ARF+IFNb) PDOTS data is highlighted in red. (G) IFNb expression in PDOTS supernatant (n = 4) after 5 days of treatment compared to 100 ng/mL of recombinant human IFNb. (H) Fluorescence microscopy of nuclear ARF protein expression in melanoma PDOTS treated for 5 days on-chip. Scale bar = 20 μm. One-way ANOVA and Welch's t test. $^{**}p < 0.001$ and ns, not significant.

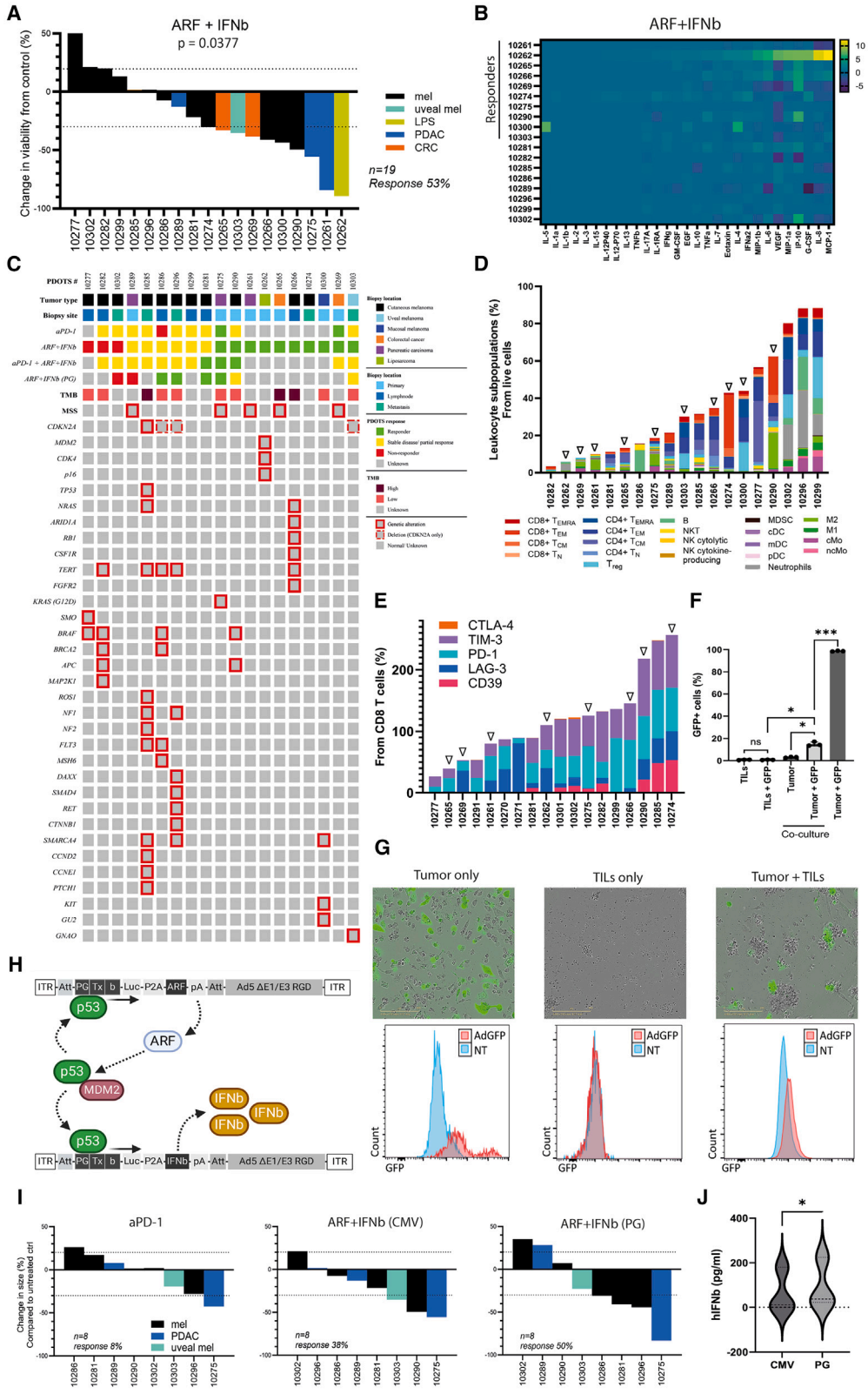

(legend on next page)

modulation and not the vector or underlying antiviral responses. Tumors excised from mice treated *in situ* with ARF+IFNb showed a timid increase in PD-L1 transcript levels and significant upregulation of PD-L1 surface expression 72 h after the last treatment (Figures 3D, 3E, and S2A). As PD-L1 overexpression is known to induce immune evasion,[16,17] we combined the gene therapy with PD(L)1 checkpoint inhibitors (Figure 3F). In a checkpoint-blockade-resistant model (B16F10 [B16] tumors), the combination of gene therapy and immune checkpoint inhibitors (ICIs) was not cooperative, with no increase in survival or superior tumor growth control as compared to the gene therapy alone (Figures 3G–3J). However, as observed with PDOTS, the response to the gene therapy alone on ICI-resistant tumors was highly efficient, with more than half the individuals responding to ARF+IFNb (Figure 3J). In the checkpoint-blockade-sensitive MC38 model, no cooperation was observed either, as animals responded well and similarly to both therapies (Figure S3). To help understand why no cooperation was observed in the B16 model, blood, spleens, and tumors excised from mice treated with ARF+IFNb and anti-PD-1 were analyzed (Figures 3K and S2B). A significant increase in IFN gamma (IFNg) in the sera of ARF+IFNb+anti-PD-1 was observed compared to the untreated mice, with no significant alteration in other cytokine sera levels among the conditions (Figures 3L and S2C). The gene therapy effectively killed the tumor cells without compromising infiltrated immune cells (Figures 3M and 3N). Even though a decrease of $CD8^+$ T cells was observed in both the spleen and tumors of treated mice, the *ex vivo* proliferation of naive splenocytes co-cultured with tumor cells treated with ARF+IFNb was robust and markedly greater than that of untreated tumors (Figures S2D–S2F). Nonetheless, tumor $CD8^+$ T cell populations were not altered when cell count was normalized to tumor volume, indicating that this decrease was instead associated with tumor shrinkage (Figure 3O). In addition, an increase of innate immune cells, notably myeloid and natural killer (NK) cells, was observed in tumors of animals treated with the gene therapy (Figure 3O). In a parallel cohort of PDOTS to that of Figure 2A, 12 PDOTS were treated on chip with ARF+IFNb in combination with anti-PD-1, and once again, no significant cooperation was observed, even though a screening of human melanoma cell lines showed the upregulation of PD-L1 upon treatment with ARF+IFNb (Figures 3P, S4, and S5). One melanoma PDOTS was treated and co-cultured with autologous peripheral blood mononuclear cells (PBMCs) in a 96-well plate, and after 5 days, the leukocytes were analyzed for immune checkpoint pathway modulation upon therapy. In addition to PD-1, the inhibitory receptor LAIR-1 was also upregulated, and the stimulatory receptor NKG2D was downregulated (Figure 3Q). Together, these results indicate that even though PD-1 and PD-L1 are upregulated upon treatment, the combination of gene therapy and checkpoint blockade does not improve the response, suggesting that lymphoid cells may not be the main mediators of the response to gene therapy, but rather innate immune cells.

Gene therapy with ARF+IFNb induces M1 polarization of monocytes in melanoma and PDAC human models

As the results of the previous sections showed that the ARF+IFNb gene therapy induces the overexpression of myeloid-attracting cytokines in the tumor, works best with colder and innate immune cell-infiltrated tumors, and tends to increase myeloid populations in the tumor, we tested whether monocytes co-cultured with treated tumor spheroids would polarize toward M1 or M2 macrophage phenotypes (Figure 4A). A375 spheroids seeded on a gel bed were efficiently transduced by the vectors and decreased in size after treatment, shrinking or disappearing when co-cultured with monocytes (Figures 4B–4D). Four days following co-culture with treated spheroids, the monocytes polarized toward M1 phenotypes and produced more interleukin (IL)-8, a macrophage-attracting chemokine overexpressed by M1 macrophages (Figures 4E and 4F).[18] In a pancreatic cancer model using GFP^+ AsPC-1 cells, similar results were observed, with an even more significant reduction in spheroid size upon treatment, an increase of M1- and a decrease of M2-polarized macrophages, and higher levels of IL-8 in the ARF+IFNb condition (Figures 4G–4I and S6). These data confirm the important antitumoral role of myeloid cells in the response to the gene therapy.

DISCUSSION

Here, we demonstrate that PDOTS represent a valuable and clinically relevant model for testing candidate viral-vector-based gene therapies in cancer. Our findings indicate that combined gene therapy using ARF and IFNb is a promising strategy, particularly for tumors that are often unresponsive to checkpoint inhibitors and other therapeutic modalities.

In previous studies, we demonstrated that when combined with IFNb, the ARF protein, which restores p53 pathway function, induces tumor cell death with apoptosis, necroptosis, and immunogenic cell death

Figure 2. Gene therapy with adenoviral vectors in patient-derived models

(A) PDOTS from 19 patients were treated on chip with 2×10^7 TU of ARF+IFNb ($n = 3$ biological replicates for each PDOTS) and analyzed for changes in spheroid viable area by fluorescence microscopy. The dashed lines indicate the responders (>30% decrease in viable area relative to untreated control), non-responders (>20% growth relative to untreated control), and partial responders (in between). (B) Cytokine levels in the conditioned media of PDOTS expressed as log2 fold change (L2FC) of ARF+IFNb relative to the untreated control. (C–E) Analyses of untreated patient tumors used for the PDOTS: (C) tumor histological type; tumor type (location); PDOTS response to aPD-1 alone, ARF+IFNb under CMV promoter, aPD-1+ARF+IFNb (CMV), or ARF+IFNb under PG promoter; tumor mutational burden (TMB); and tumor mutations of specimens used for PDOTS profiling ($n = 19$). (D and E) Baseline immunophenotyping with 22 immune subpopulations identified from the viable cells (D) and CD8 T cell exhaustion markers (E) in patient tumor specimens used for PDOTS. (F and G) GFP+ cells (F) and GFP expression (G) in melanoma 10,049 cells and autologous TILs treated alone or co-cultured (4:1) for 5 days with GFP control vector. (H) Schematic of collaboration between ARF and IFNb vectors under p53-responsive promoter PG. (I and J) Change in spheroid viable area (I) and IFNb expression (J) in conditioned media after PDOTS treatment with ARF+IFNb under CMV or PG promoters. One-way ANOVA and Welch's t test. One-sided, paired, Wilcoxon test for waterfall plots. $^*p < 0.05$, $^{***}p < 0.001$, and ns, not significant. Mel, melanoma; uveal mel, uveal melanoma; CRC, colorectal cancer; PDAC, pancreatic ductal adenocarcinoma; LPS, liposarcoma.

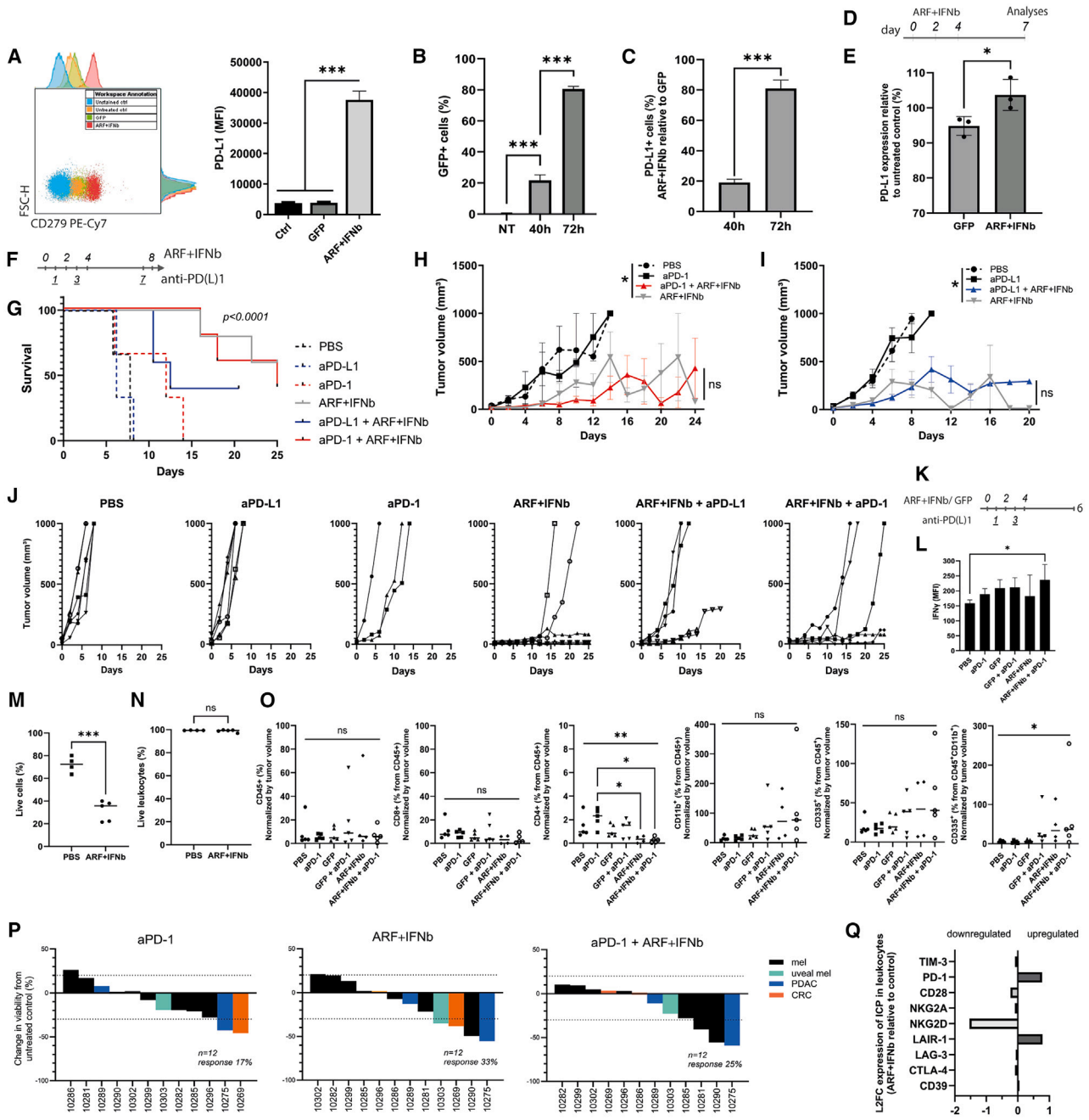

Figure 3. ARF+IFNb and PD-1/PD-L1 modulation in mouse and human models

(A) B16 cells transduced with adenoviral vectors (final MOI: 1,000) were analyzed for PD-L1 expression by flow cytometry. (B and C) Alternatively, the time-dependent transgene expression was assessed using the GFP coding vector (B) and compared to time-dependent PD-L1 expression upon *in vitro* treatment with ARF+IFNb (C). (D and E) C57BL/6J mice ($n = 3$) with subcutaneous B16 tumors were treated intratumorally with adenoviral vectors (1×10^9 TU) on days 0, 2, and 4 and euthanized by day 7 (D) for analysis of PD-L1 protein surface expression in excised tumors (E). (F) Subsequently, mice were treated with a combination of ARF+IFNb vectors on days 0, 2, 4, and 8 and anti-PD-(L)1 antibodies on days 1, 3, and 7. (G and H) Survival (G) and mean tumor volume (H) of ARF+IFNb+anti-PD-1 (I) or ARF+IFNb+anti-PD-L1 were assessed. (J) Individual tumor volume per treatment condition is also shown. (K) To analyze treatment immune effects, mice were treated on days 0, 2, and 4 with ARF+IFNb or GFP and/or with anti-PD-1 on days 1 and 3 and euthanized by day 6. (L and M) Blood was collected for sera cytokine measurement and tumors were excised and processed for the assessment of (M) total live cells, (N) live leukocytes, and (O) immunophenotyping. Total leukocyte (CD45+), CD8 T cell, CD4 T cell, innate immune/mostly myeloid cell (CD11b+), NK cell (CD335+), and mature NK cell (CD335+ CD11b+) populations were analyzed. (P) Twelve patient tumors were processed fresh to establish and treat PDOTS with anti-PD-1 alone or in combination with ARF+IFNb and analyzed for changes in spheroid viable area. (Q) One melanoma PDOTS co-cultured with autologous

(legend continued on next page)

features.[5,6,8] Building on this, our current work further elucidates underlying immune mechanisms triggered by this gene therapy, revealing a significant increase in innate immune-cell-attracting cytokines within the tumor microenvironment (TME) and the polarization of monocytes toward an M1 phenotype in human models. These results were predictable, as both viral vectors and type I IFNs are established inducers of innate immune responses.[19]

Notably, the PDOTS with the strongest therapeutic response and the most pronounced increase in cytokine expression from the cohort analyzed was the retroperitoneal liposarcoma specimen. These tumors, originating from the fat tissue, are genetically characterized by WT *TP53* and chromosomal amplification of *MDM2*, resulting in an impaired p53 pathway due to MDM2-mediated degradation of the tumor-suppressor protein.[20,21] This genetic profile, coupled with ARF's role in counteracting MDM2-mediated degradation of p53, justifies the status of the liposarcoma as the most responsive specimen to ARF+IFNb therapy.

Importantly, we observed that the status of *CDKN2A* was an important determinant of response in the eight treated PDOTS treated with the p53-responsive promoter PG in comparison to the constitutive promoter CMV. These findings suggest the potential for a more personalized application of ARF+IFNb gene therapy, particularly for tumors known to carry this specific genetic profile, such as liposarcomas.

Despite the PD-L1 upregulation identified upon gene transfer, no cooperation was observed when associating the gene therapy with checkpoint inhibitors. Similarly, the MASTERKEY-265 (ClinicalTrials.gov: NCT02263508) phase 3 clinical trial testing the combination of T-VEC, an FDA-approved viral vector gene therapy for melanoma, with anti-PD-1 showed no significant improvement in overall survival (OS) or progression-free survival (PFS).[22] As observed in our study, PD-L1 upregulation has been detected on responsive tumors upon treatment with T-VEC due to type I IFN production in the infected cells.[23,24] The phase 1b clinical trial testing the combination of T-VEC and anti-PD-1 showed that tumors with low $CD8^+$ cell density, which has a negative prediction value for anti-PD-1 response, responded to the treatment, which may explain why no cooperation was observed in the expanded cohort of the phase 3 clinical trial.[23,25]

The lack of cooperation observed for ARF+IFNb and anti-PD-1 may also be due to an antiviral instead of an antitumor response induced by the gene therapy. A similar case was recently reported by Webb and colleagues,[26] in which an oncolytic vesicular stomatitis virus (VSV) encoding IFNb in combination with anti-PD-1 did not show cooperation. Yet, when the vector encoded both IFNb and tumor antigens, cooperation with anti-PD-1 was seen and correlated with an increase in tumor-specific CD8 T cells.[26] Thus, improving the gene therapy approach to redirect the T cell response to tumor antigens may provide the opportunity for cooperation with checkpoint blockade, making this approach suitable for a different set of patients.

Other reasons for the ineffective combination may include the choice of treatment regimen, not allowing enough time for the gene therapy to take effect before boosting the immune response with pembrolizumab, sample size, and clinical context.[25,27] Two ongoing trials (ClinicalTrials.gov: NCT04068181 and NCT04330430) testing the combination of T-VEC and anti-PD-1 in the neoadjuvant setting for melanomas are showing cooperation in patients who previously failed on anti-PD-1.[28,29] Similarly, we observed in our cohort that combining ARF+IFNb and anti-PD-1 was, to some extent, successful for a subset of melanomas, suggesting that the examination of a larger cohort may bring the statistical significance necessary to identify patients who could benefit from the combination.

Taken together, our findings underscore the potential of ARF+IFNb therapy, particularly in treating liposarcoma and other tumors with low T cell and immune cell density and impaired p53 pathways due to ARF-MDM2 imbalances. Furthermore, they strongly support the use of PDOTS as a platform for evaluating gene therapy strategies in cancer. Future studies should focus on elucidating the precise immune interactions at play and exploring the potential of ARF+IFNb in genetically defined patient subsets and potential combinations.

MATERIALS AND METHODS

Patient samples

Tumor samples from a cohort treated at Massachusetts General Hospital (MGH) (September 2022–August 2023) were used to establish PDOTS. Samples were collected under protocols approved by the Dana-Farber/Harvard Cancer Center (DF/HCC) institutional review board (IRB), and de-identified data were obtained from the MGH Melanoma Blood and Tissue Repository. Written informed consent was obtained from all subjects. These studies were conducted according to the Declaration of Helsinki and approved by the DF/HCC IRB. Mutational analyses were performed via next-generation sequencing or immunohistochemistry at MGH. Clinical response was defined as an OS > 360 days and a PFS > 180 days. Peripheral blood from two healthy donors was collected at the Cancer Institute of São Paulo (ICESP) under ethics-approved guidelines.

Cell culture

Cell lines B16, A375, UACC-62, and SK-MEL-5 were cultured in Roswell Park Memorial Institute (RPMI)-1640 medium (Thermo Fisher Scientific, Waltham, MA, USA) supplemented with 10% fetal bovine serum (FBS) and 1% antibiotic-antimycotic (100×; Thermo Fisher Scientific). 293A, SK-MEL-29, SK-MEL-19, SK-MEL-147, GFP+

PBMCs in a 96-well plate and treated for 5 days with ARF+IFNb was immunophenotyped to assess log2 fold change (L2FC) of immune checkpoint (ICP) receptor expression in leukocytes in the treated condition relative to the untreated control. One-way ANOVA, Brown-Forsythe test, and Student's t test. Log rank (Mantel-Cox) test for survival analysis. One-sided, paired, Wilcoxon test for waterfall plots. *$p < 0.05$, **$p < 0.01$, ***$p < 0.001$, ****$p < 0.0001$, and ns, not significant. Mel, melanoma; uveal mel, uveal melanoma; CRC, colorectal cancer; PDAC, pancreatic ductal adenocarcinoma.

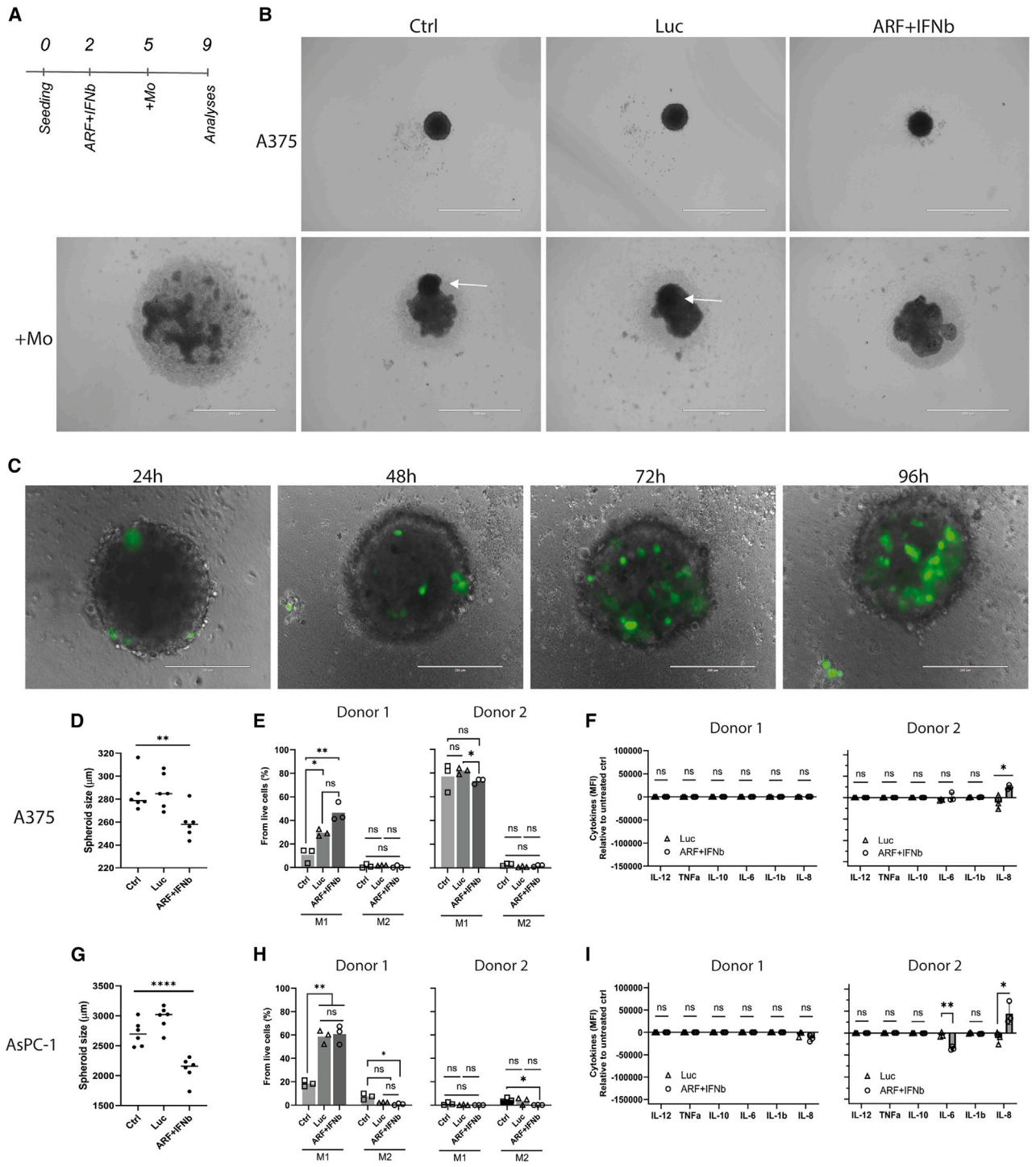

Figure 4. Polarization of monocytes co-cultured with cell line spheroids treated with ARF+IFNb

(A) A375 cells were plated on an agarose bed in a 96-well plate. After 48 h, the spheroids were treated with ARF+IFNb or Luc at a final MOI of 200. After 72 h of treatment, monocytes (Mo) isolated from the PBMCs of two healthy donors were added to separate wells at a 5:1 ratio. (B) The treated spheroids were imaged by optical microscopy (4× magnification) on day 9 (white arrow = spheroids). Scale bar = 1000 µm. (C) Alternatively, spheroids were transduced with the control GFP vector and imaged for 5 days every

(legend continued on next page)

AsPC-1, and PDOTS were cultured in Dulbecco's modified Eagle medium (DMEM; Thermo Fisher Scientific) supplemented as described above, with MC38 having the addition of 1 mM sodium pyruvate (Thermo Fisher Scientific). The 10049 line and autologous TILs were cultured in SmGM (Lonza, Basel, Switzerland) and ImmunoCult-XF medium (STEMCELL Technologies, Vancouver, Canada) with 50 ng/mL IL-2 (PeproTech, Cranbury, NJ), USA, respectively. Murine splenocytes were cultured *ex vivo* in RPMI medium supplemented with 10% FBS, 1% glutamine (Thermo Fisher Scientific), 0.01% beta-mercaptoethanol (Thermo Fisher Scientific), and 0.5 U/mL DNase I (Roche, Basel, Switzerland). All cultures were maintained at 37°C, 5% CO_2.

Large-scale production of adenoviral vectors

All vectors in this study are adenoviral vectors (Ad) serotype 5, modified with the RGD tripeptide motif in the H1 loop of the fiber knob.[30] All murine vectors bear the p53-responsive promoter PG previously constructed.[31] Human vectors bear the constitutive CMV promoter unless specified otherwise and encode the reporter gene Luciferase (Luc) in addition to the therapeutic genes ARF and IFNb. The vectors were constructed as previously described.[5,6,8] Briefly, a plasmid backbone (kindly provided by Dr. Hiroyuki Mizuguchi from Osaka University, Japan) was modified for *in vitro* recombination using the LR Clonase II enzyme (Invitrogen, 12538120). The adenoviral vector plasmids containing the respective transgenes and promoters (Figure S7) were linearized and transfected into 293A cells for multiple amplification cycles to obtain the viral vectors. The viruses were produced as detailed previously.[32] Briefly, 25 150 mm plates containing 293A producer cells infected with the vectors were collected when an approximately 50% cytopathic effect was observed. The cells were lysed, and the lysate was centrifuged for iodixanol gradient separation of the vector-containing band. Its content was purified using PD-10 columns (Sigma, Burlington, MA, USA) following the manufacturer's instructions. The purified vectors were aliquoted, stored in PBS with 7% glycerol, and kept at −80°C until use. The biological titer of each virus was determined using the Adeno X-Rapid titer kit, following the manufacturer's instructions (Takara Bio, Mountain View, CA, USA).

In vitro gene transfer

For the transduction of murine and human tumor cells *in vitro*, the respective culture medium and supplements for each cell line were used as described above. Cells were plated in 12- or 24-well plates and treated in suspension with the vectors according to the multiplicity of infection (MOI), which is the ratio of viral particles to the number of cells, as detailed in the legend of each figure. The treatment was conducted using half of the total well volume, with the remaining culture medium added after 4 h of incubation.

In vivo mouse models

C57BL/6J mice (6 weeks old, male) were obtained from the Animal Facility Center of the Faculty of Medicine, University of São Paulo (FMUSP). All animals were maintained under specific pathogen-free (SPF) conditions with access to food and water *ad libitum*. All procedures and conditions were approved by the Animal Ethics Committee (CEUA, FMUSP). Mice were subcutaneously (s.c.) inoculated with 1 or 7 × 10^5 B16 or MC38 cells, respectively, in PBS for a final volume of 100 μL. When the tumors reached 3 × 3–4 × 4 mm, they were treated intratumorally with 1 × 10^9 ARF + 1 × 10^9 IFNb or 2 × 10^9 GFP in PBS (all vectors with the PG promoter, number of transducing units (TU) indicated) for a final volume of 50 μL, or with PBS alone, on the days indicated in the figure legends. When specified, animals were treated intraperitoneally (i.p.) with 100 μg of anti-PD-1 monoclonal antibody (clone RMP1, BioXCell) or anti-PD-L1 (clone 10F.9G2, BioXCell) in a final volume of 200 μL, diluted according to the manufacturer's instructions. Tumor volume was measured with a digital caliper every 48 h and calculated using the formula $V(mm^3) = (d^2 \times D)/2$ (where V is the tumor volume, d is the smaller diameter, and D is the larger diameter). The animals were anesthetized with isoflurane inhalation and euthanized in a CO_2 chamber on the day indicated in the figure legends or earlier if tumor ulceration was observed.

On-chip MTS and PDOTS

MTS and PDOTS were prepared from tumor cell lines and fresh patient tumor samples. For MTS, 1 million cells were added to an ultra-low attachment T-75 flask (Corning, New York, NY, USA) in 10 mL of their respective culture medium and incubated for 48 h at 37°C to allow spheroid formation. The subsequent steps of MTS preparation and treatment were the same as those for PDOTS, as previously described.[33] The vectors were added to the spheroid-collagen mix at 2 million total TU for each device (r = 1, 10 μL). One AIM Dax-01 chip (AIM Biotech, Singapore) with three devices (biological replicates) was used for each MTS or PDOTS. When specified, anti-PD-1 (250 μg/mL pembrolizumab) was mixed with the culture media and added to the side channels of the chips containing the PDOTS. Otherwise, only media were added upon gel polymerization. The culture medium in the devices was not replaced or replenished during the incubation period at 37°C with 5% CO_2 for up to 7 days. After the incubation period, the conditioned medium was stored at −80°C for cytokine analysis, and the chips were stained for fluorescence microscopy.

Fluorescence microscopy

The cell viability of MTS and PDOTS was analyzed as previously described.[33] Quantification involved binary measurement of dye-positive areas and Ho-PI (live cells), with data presented as log2 fold change (L2FC) relative to controls. For p14ARF analysis in PDOTS,

24 h (20× magnification) for GFP detection. (D and E) The diameter of treated A375 spheroids was measured (n = 6 per condition) (D) and the cells were subsequently collected and analyzed for differentiation of monocytes into M1 macrophages (M1, CD80+CD163-) or M2 macrophages (M2, CD163+) (E) and cytokine expression on conditioned media after 4 days of treatment (F). (G–I) The pancreatic cancer cell line AsPC-1 transformed to express GFP constitutively was similarly treated, and (G) spheroid size, (H) monocyte polarization, and (I) cytokine levels were assessed. One-way ANOVA and multiple t tests with Welch correction. $^*p < 0.05$, $^{**}p < 0.01$, and $^{***}p < 0.001$.

the conditioned medium was replaced with 200 μL of 4% paraformaldehyde (PFA) in PBS, incubated for 15 min at room temperature, and then replaced with 0.1% Triton X-100 in PBS for 10 min. After washing, samples were blocked with 5% FBS in PBS for 1 h, followed by incubation with primary anti-p14ARF antibody (1:100) at 4°C for 16 h. After washing, the secondary antibody (Alexa Fluor 647, 1:500) was added and incubated for 2–4 h. PDOTS were then stained with Hoechst and imaged using the Thunder microscope (20× magnification). For real-time GFP transduction analysis in 10049 cells co-cultured with TILs, the Incucyte system was used, with images taken on day 5. Spheroids co-cultured with monocytes were photographed at specified time points using the EVOS microscope at 4× and 20× magnifications. Diameter analysis was performed using ImageJ.

Co-culture of tumor cells with immune cells

B16 cells were transduced *in vitro* with vectors at an MOI of 1000. After 40 h, half of the medium was replaced, and pre-activated splenocytes were added at a 10:1 ratio. Splenocytes were obtained by dissociating a spleen from a tumor-free animal, lysing red blood cells with homemade ACK buffer, and pre-activating with PMA and ionomycin. For lymphocyte proliferation assays, splenocytes were labeled with Cell Trace CFSE and then added to B16 cells treated with ARF+ IFNb and anti-PD-1. After 72 h, non-adherent cells were collected for flow cytometry. For co-culture of 10049 cells with TILs, 2,000 cells were plated, and then 10,000 TILs and vectors (MOI 50) were added after 24 h. The plate was incubated in the Incucyte system. For PDOTS co-cultured with PBMCs, the collagen concentration was reduced to 1.7 mg/mL, and PBMCs were added in a 1:1 ratio in DMEM with 10% FBS. The plate was incubated for 5 days, and both supernatant and spheroids were collected for flow cytometry.

Cell line spheroids on gel bed

10,000 A375 or GFP+ AsPC-1 cells in 200 μL of DMEM with 10% FBS were plated in 96-well round-bottom plates on a 1% agarose gel bed in PBS (50 μL per well) to form spheroids, as previously described.[34] After 2 days, two-thirds of the medium was removed and replaced with fresh medium containing 5 and 15 × 10^5 TU ARF and IFNb or Luc, respectively, carefully added to the side of the wells. After 4 h, the volume was adjusted with fresh medium to 200 μL. Following 72 h of incubation, peripheral blood from two healthy donors was collected in EDTA tubes, diluted in PBS, and processed via density gradient centrifugation with Ficoll-Plaque Plus (GE Healthcare, UK). The cells were resuspended in 10 mL serum-free RPMI and incubated for 2 h at 37°C. After incubation, the cells were treated with TrypLE express enzyme (Gibco, Waltham, MA, USA) and collected, and adherent cells were scraped off. 50,000 monocytes were added to the spheroids after removing half of the conditioned medium. After 4 days, the spheroids were examined by fluorescence microscopy, the culture medium and spheroids were collected and centrifuged, and the conditioned medium was stored at −80°C for cytokine analysis. The cells were resuspended, incubated with TrypLE, washed with PBS containing 2% FBS, and prepared for flow cytometry.

Cytokine detection assays

A cardiac puncture was performed on anesthetized animals for cytokine concentration analysis in the serum of treated animals. After blood collection, the animals were euthanized in a CO_2 chamber. The blood was allowed to clot and then centrifuged at 250 × *g* for 10 min at 4°C to separate the serum, which was stored frozen at −80°C until analysis. For the analysis, 100 μL of serum was used with the mouse Th1/Th2/Th17 CBA kit (BD Biosciences, San Jose, CA, USA), and another 100 μL was used with the murine IFNβ ELISA kit (R&D Systems, Minneapolis, MN, USA), following the manufacturer's instructions. The supernatants from spheroids co-cultured with monocytes were frozen and analyzed for human cytokine concentrations using the human inflammatory cytokine CBA kit (BD Biosciences) and the human IFNβ ELISA kit (R&D Systems). The conditioned medium from PDOTS was preserved at −80°C and analyzed (25 μL, undiluted) for secreted cytokine concentrations (pg/mL) using the Milliplex MAP human cytokine/chemokine magnetic bead panel (Merck Millipore, Burlington, MA, USA) according to the manufacturer's instructions.

Flow cytometry

Various analyses were conducted using flow cytometry, with antibody details listed in Table S1. Cells were stained with 1 μL of LIVE/DEAD dye (Thermo Fisher Scientific) in 1 mL Hank's buffer (with DNase I), using 100 μL per sample (1–10 × 10^5 cells). After 30 min of incubation at room temperature in the dark, the cells were washed twice with buffer containing 5% FBS and then centrifuged at 300 (tumor cells) or 15,000 (immune cells) × *g*. Pellet cells had their Fc receptors blocked with the Human TruStain FcX solution (BioLegend, San Diego, CA, USA) for 5–10 min at room temperature. Surface antibodies were added to 25–100 μL final volume (1 × 10^5–2 × 10^6 cells) and incubated at 4°C for 30 min. Samples were washed and fixed with 4% PFA for 20 min at 4°C and stored in Hank's buffer for analysis within 5 days. For *in vivo* immunophenotyping, excised tumors were processed with collagenases, filtered, and stained with antibodies after LIVE/DEAD staining. Patient-derived samples and PDOTS were analyzed fresh, with fluorescence minus one controls used. The Attune NxT flow cytometer was used for mouse cell lines, BD LSRFortessa X-20 for other murine assays and spheroids + monocytes, and Northern Lights spectral cytometer for other human cells. Data were analyzed using FlowJo software.

RT-qPCR

For quantitative reverse-transcritpion PCR, tumors were dissociated, a total of 1 million cells were collected in 0.3 mL of TRIzol (Thermo Fisher Scientific), and RNA was extracted using chloroform and isopropanol according to the manufacturer's instructions. RNA was subsequently treated with DNase I (Roche) at room temperature for 15 min. The RNA concentration was determined by measuring absorbance at 260 nm. The primer sequences used for human PD-L1 are 5'-CCTGCTGTCACTTGCTACG-3' (forward) and 5'-GGGAATCT GCACTCCATCGT-3' (reverse), and for GAPDH, they are 5'-CAGC AACTCCCACTCTTCC-3' (forward) and 5'-CCATGTAGGCCATG AGGTTC-3' (reverse). Total RNA (100 ng) was used for quantitative

PCR using the GoTaq 1-Step RT-qPCR System (Promega, Madison, WI, USA). Amplification conditions consisted of reverse transcription at 37°C for 15 min and denaturation at 95°C for 15 min, followed by 40 cycles of denaturation at 95°C for 10 s, annealing at 60°C for 30 s, and extension at 72°C for 30 s. Samples were tested in technical triplicates and analyzed using 7500 Fast software, v.2.05 (Applied Biosystems, Foster City, CA, USA). Gene expression was normalized to the endogenous GAPDH gene and expressed as fold increase using the $2 - \Delta\Delta Ct$ method.

Statistical and data analyses

The statistical tests and biological replicates for each analysis are specified in the figure legends and/or text. Data are presented as mean ± SD except in tumor volume progression and survival graphs, where data are shown as mean ± SEM. Statistical differences between groups are indicated as not significant (ns, $p > 0.05$) or significant, with $^{*}p < 0.05$, $^{**}p < 0.01$, $^{***}p < 0.001$, and $^{****}p < 0.0001$. Statistical analyses were performed using Prism GraphPad v.10.2.2.

DATA AND CODE AVAILABILITY

Data generated by the authors are available upon request.

ACKNOWLEDGMENTS

We thank Mara de Souza Junqueira (Centro de Medicina Nuclear-FMUSP) for assistance with the *in vivo* studies. We appreciate the efforts of Dr. Roger Chammas and his group (ICESP-FMUSP) for continued collaboration and valuable discussions. This work was supported by the São Paulo Research Foundation: fellowships 18/25555-9 and 22/04368-1 (A.C.M.D.), 2017/25290-2 (N.G.T.), and 17/25284-2 (O.R.) and grants 15/26580-9 and 22/15913-0 (B.E.S.). Funding was also provided by the Conselho Nacional de Desenvolvimento Cientifico e Tecnológico through fellowship 310497/2021-3 and grant 401811/2024-7 (B.E.S.). This study was financed in part by the Coordenação de Aperfeiçoamento de Pessoal de Nível Superior - Brasil (CAPES) - Finance Code 001 (S.B.d.O.). We also acknowledge support for the MGH Tumor Cartography Center through the Massachusetts Life Sciences Center Research Infrastructure Program. The graphical abstract and Figures 1D, 2H, and S8 were created with Biorender.com using a paid license.

AUTHOR CONTRIBUTIONS

Conception and experimental design, A.C.M.D., S.B.d.O., N.G.T., A.P.L., S.C., R.W.J., and B.E.S.; methodology and data acquisition, A.C.M.D., S.B.d.O., N.G.T., A.P.L., O.R., R.W.J., and B.E.S.; analysis and interpretation of data, A.C.M.D., S.B.d.O., N.G.T., A.P.L., S.C., R.W.J., and B.E.S.; administrative, technical, or material support, A.P.L., T.S., A.L., D.L., M.B., and G.M.B.; manuscript writing and revision, A.C.M.D., A.P.L., R.W.J., and B.E.S.

DECLARATION OF INTERESTS

The authors declare no competing interests.

SUPPLEMENTAL INFORMATION

Supplemental information can be found online at https://doi.org/10.1016/j.omton.2025.200942.

REFERENCES

1. Wolchok, J.D., Chiarion-Sileni, V., Gonzalez, R., Grob, J.J., Rutkowski, P., Lao, C.D., Cowey, C.L., Schadendorf, D., Wagstaff, J., Dummer, R., et al. (2022). Long-Term Outcomes With Nivolumab Plus Ipilimumab or Nivolumab Alone Versus Ipilimumab in Patients With Advanced Melanoma. J. Clin. Oncol. *40*, 127–137. https://doi.org/10.1200/JCO.21.02229/SUPPL_FILE/PROTOCOL_JCO.21.02229.PDF.

2. Mitra, A., Barua, A., Huang, L., Ganguly, S., Feng, Q., and He, B. (2023). From bench to bedside: the history and progress of CAR T cell therapy. Front. Immunol. *14*, 1188049. https://doi.org/10.3389/FIMMU.2023.1188049/BIBTEX.

3. Chancellor, D., Barrett, D., Nguyen-Jatkoe, L., Millington, S., and Eckhardt, F. (2023). The state of cell and gene therapy in 2023. Mol. Ther. *31*, 3376–3388. https://doi.org/10.1016/J.YMTHE.2023.11.001.

4. Bray Bsc, F., Laversanne, | M., Hyuna, |, Phd, S., Ferlay, J., Siegel Mph, R.L., Soerjomataram, I., Ahmedin, |, and Dvm, J. (2024). Global cancer statistics 2022: GLOBOCAN estimates of incidence and mortality worldwide for 36 cancers in 185 countries. CA Cancer J. Clin. *74*, 229–263. https://doi.org/10.3322/CAAC.21834.

5. Cerqueira, O.L.D., Clavijo-Salomon, M.A., Cardoso, E.C., Citrangulo Tortelli Junior, T., Mendonça, S.A., Barbuto, J.A.M., and Strauss, B.E. (2020). Combined p14ARF and Interferon-β Gene Transfer to the Human Melanoma Cell Line SK-MEL-147 Promotes Oncolysis and Immune Activation. Front. Immunol. *11*, 576658. https://doi.org/10.3389/FIMMU.2020.576658/BIBTEX.

6. Hunger, A., Medrano, R.F.V., Zanatta, D.B., Del Valle, P.R., Merkel, C.A., Salles, T. de A., Ferrari, D.G., Furuya, T.K., Bustos, S.O., Saito, R. de F., et al. (2017). Reestablishment of p53/Arf and interferon-β pathways mediated by a novel adenoviral vector potentiates antiviral response and immunogenic cell death. Cell Death Discovery *3*, 1–12. https://doi.org/10.1038/cddiscovery.2017.17.

7. Medrano, R.F.V., Salles, T.A., Dariolli, R., Antunes, F., Feitosa, V.A., Hunger, A., Catani, J.P.P., Mendonça, S.A., Tamura, R.E., Lana, M.G., et al. (2022). Potentiation of combined p19Arf and interferon-beta cancer gene therapy through its association with doxorubicin chemotherapy. Sci. Rep. *12*, 1–14. https://doi.org/10.1038/s41598-022-17775-y.

8. Mendonça, S.A., Antunes, F., Cerqueira, O.L.D., Del Valle, P.R., Hunger, A., Oliveira, P.V.S.D., Brito, B., Costanzi-Strauss, E., and Strauss, B.E. (2023). Induction of Immune-Stimulating Factors and Oncolysis Upon p14ARF Gene Transfer in Melanoma Cell Lines. DNA Cell Biol. *42*, 274–288. https://doi.org/10.1089/DNA.2022.0115.

9. Efe, G., Rustgi, A.K., and Prives, C. (2024). p53 at the crossroads of tumor immunity. Nat Cancer *5*, 983–995. https://doi.org/10.1038/S43018-024-00796-Z.

10. Sandoval, R., Xue, J., Pilkinton, M., Salvi, D., Kiyokawa, H., and Colamonici, O.R. (2004). Different Requirements for the Cytostatic and Apoptotic Effects of Type I Interferons: INDUCTION OF APOPTOSIS REQUIRES ARF BUT NOT p53 IN OSTEOSARCOMA CELL LINES. J. Biol. Chem. *279*, 32275–32280. https://doi.org/10.1074/JBC.M313830200.

11. Takaoka, A., Hayakawa, S., Yanai, H., Stoiber, D., Negishi, H., Kikuchi, H., Sasaki, S., Imai, K., Shibue, T., Honda, K., et al. (2003). Integration of interferon-alpha/beta signalling to p53 responses in tumour suppression and antiviral defence. Nature *424*, 516–523. https://doi.org/10.1038/NATURE01850.

12. Sun, Y., Maggs, L., Panda, A., Wright, S.J., Cicerchia, A.M., Jenney, A., Perricone, M.D., Mills, C.E., Cattaneo, G., Ventin, M., et al. (2025). TBK1 Targeting Is Identified as a Therapeutic Strategy to Enhance CAR T-Cell Efficacy Using Patient-Derived Organotypic Tumor Spheroids. Cancer Immunol. Res. *1*, OF1–OF19. https://doi.org/10.1158/2326-6066.CIR-23-1011.

13. Wang, Y., Buck, A., Piel, B., Zerefa, L., Murugan, N., Coherd, C.D., Miklosi, A.G., Johal, H., Bastos, R.N., Huang, K., et al. (2024). Affinity fine-tuning anti-CAIX CAR-T cells mitigate on-target off-tumor side effects. Mol. Cancer *23*, 1–16. https://doi.org/10.1186/S12943-024-01952-W/FIGURES/6.

14. Cheon, H.J., Wang, Y., Wightman, S.M., Jackson, M.W., and Stark, G.R. (2023). How cancer cells make and respond to interferon-I. Trends Cancer *9*, 83–92. https://doi.org/10.1016/j.trecan.2022.09.003.

15. Thiem, A., Hesbacher, S., Kneitz, H., Di Primio, T., Heppt, M.V., Hermanns, H.M., Goebeler, M., Meierjohann, S., Houben, R., and Schrama, D. (2019). IFN-gamma-induced PD-L1 expression in melanoma depends on p53 expression. J. Exper. Clin. Cancer Res. *38*, 1–15. https://doi.org/10.1186/S13046-019-1403-9/FIGURES/5.

16. Dong, H., Strome, S.E., Salomao, D.R., Tamura, H., Hirano, F., Flies, D.B., Roche, P.C., Lu, J., Zhu, G., Tamada, K., et al. (2002). Tumor-associated B7-H1 promotes T-cell apoptosis: a potential mechanism of immune evasion. Nat. Med. *8*, 793–800. https://doi.org/10.1038/NM730.

17. Hanahan, D. (2022). Hallmarks of Cancer: New Dimensions. Cancer Discov. *12*, 31–46. https://doi.org/10.1158/2159-8290.CD-21-1059.

18. Meniailo, M.E., Malashchenko, V.V., Shmarov, V.A., Gazatova, N.D., Melashchenko, O.B., Goncharov, A.G., Seledtsova, G.V., and Seledtsov, V.I. (2018). Interleukin-8 favors pro-inflammatory activity of human monocytes/macrophages. Int. Immunopharmacol. *56*, 217–221. https://doi.org/10.1016/J.INTIMP.2018.01.036.

19. Shirley, J.L., de Jong, Y.P., Terhorst, C., and Herzog, R.W. (2020). Immune Responses to Viral Gene Therapy Vectors. Mol. Ther. *28*, 709–722. https://doi.org/10.1016/J.YMTHE.2020.01.001.

20. Lu, J., Wood, D., Ingley, E., Koks, S., and Wong, D. (2021). Update on genomic and molecular landscapes of well-differentiated liposarcoma and dedifferentiated liposarcoma. Mol. Biol. Rep. *48*, 3637–3647. https://doi.org/10.1007/S11033-021-06362-5/METRICS.

21. Pilloti, S., Torre, G.D., Lavarino, C., Palma, S.D., Sozzi, G., Minoletti, F., Rao, S., Pasquini, G., Azzarelli, A., Rilke, F., et al. (1997). Distinct mdm2/p53 expression patterns in liposarcoma subgroups: Implications for different pathogenetic mechanisms. J. Pathol. *181*, 14–24. https://doi.org/10.1002/(SICI)1096-9896(199701)181:1<14::AID-PATH730>3.0.CO;2-O.

22. Chesney, J.A., Ribas, A., Long, G.V., Kirkwood, J.M., Dummer, R., Puzanov, I., Hoeller, C., Gajewski, T.F., Gutzmer, R., Rutkowski, P., et al. (2023). Randomized, Double-Blind, Placebo-Controlled, Global Phase III Trial of Talimogene Laherparepvec Combined with Pembrolizumab for Advanced Melanoma. J. Clin. Oncol. *41*, 528–540. https://doi.org/10.1200/JCO.22.00343/SUPPL_FILE/PROTOCOL_JCO.22.00343.PDF.

23. Ribas, A., Dummer, R., Puzanov, I., VanderWalde, A., Andtbacka, R.H.I., Michielin, O., Olszanski, A.J., Malvehy, J., Cebon, J., Fernandez, E., et al. (2017). Oncolytic Virotherapy Promotes Intratumoral T Cell Infiltration and Improves Anti-PD-1 Immunotherapy. Cell *170*, 1109. https://doi.org/10.1016/J.CELL.2017.08.027.

24. Bommareddy, P.K., Shettigar, M., and Kaufman, H.L. (2018). Integrating oncolytic viruses in combination cancer immunotherapy. Nat. Rev. Immunol. *18*, 498–513. https://doi.org/10.1038/S41577-018-0014-6.

25. Kaufman, H.L., Shalhout, S.Z., and Iodice, G. (2022). Talimogene Laherparepvec: Moving From First-In-Class to Best-In-Class. Front. Mol. Biosci. *9*, e834841. https://doi.org/10.3389/FMOLB.2022.834841.

26. Webb, M.J., Sangsuwannukul, T., van Vloten, J., Evgin, L., Kendall, B., Tonne, J., Thompson, J., Metko, M., Moore, M., Chiriboga Yerovi, M.P., et al. (2024). Expression of tumor antigens within an oncolytic virus enhances the anti-tumor T cell response. Nat. Comm. *15*, 1–18. https://doi.org/10.1038/s41467-024-49286-x.

27. Cohen, S., and Boland, G.M. (2022). Harnessing the Potential of Combination Immunotherapy and Oncolytic Virotherapy for Solid Tumors. Ann. Surg. Oncol. *29*, 762–763. https://doi.org/10.1245/S10434-021-11059-X/METRICS.

28. Gastman, B., Robert, C., Gogas, H., Rutkowski, P., Long, G.V., Chaney, M.F., Joshi, H., Lin, Y.-L., Snyder, W., and Chesney, J.A. (2022). Primary analysis of a phase 2, open-label, multicenter trial of talimogene laherparepvec (T-VEC) plus pembrolizumab (pembro) for the treatment (Tx) of patients (pts) with advanced melanoma (MEL) who progressed on prior anti–PD-1 therapy: MASTERKEY-115. J. Clin. Oncol. *40*, 9518. https://doi.org/10.1200/JCO.2022.40.16_SUPPL.9518.

29. Zijlker, L.P., van Houdt, W.J., Stahlie, E.H.A., Franke, V., Rohaan, M.W., Delatzakis, A., Zuur, C., Klop, W.M.C., van de Wiel, B.A., Kuijpers, A., et al. (2023). Neoadjuvant T-VEC + nivolumab combination therapy for resectable early metastatic (stage IIIB/C/D-IV M1a) melanoma with injectable disease: NIVEC trial. J. Clin. Oncol. *41*, 9546. https://doi.org/10.1200/JCO.2023.41.16_SUPPL.9546.

30. Mizuguchi, H., Koizumi, N., Hosono, T., Utoguchi, N., Watanabe, Y., Kay, M.A., and Hayakawa, T. (2001). A simplified system for constructing recombinant adenoviral vectors containing heterologous peptides in the HI loop of their fiber knob. Gene Ther. *8*, 730–735. https://doi.org/10.1038/SJ.GT.3301453.

31. Bajgelman, M.C., and Strauss, B.E. (2008). Development of an adenoviral vector with robust expression driven by p53. Virology *371*, 8–13. https://doi.org/10.1016/j.virol.2007.11.015.

32. Peng, H.H., Wu, S., Davis, J.J., Wang, L., Roth, J.A., Marini, F.C., and Fang, B. (2006). A rapid and efficient method for purification of recombinant adenovirus with arginine-glycine-aspartic acid-modified fibers. Anal. Biochem. *354*, 140–147. https://doi.org/10.1016/J.AB.2006.04.032.

33. Domingues, A.C.M., Palin, C., Sun, Y., Xie, H., Woods, E.C., Jenkins, R.W., and Revach, O.Y. (2024). Preparation and analysis of monotypic and organotypic tumor spheroids. Methods Cell Biol. *1*, 1. https://doi.org/10.1016/BS.MCB.2024.11.003.

34. Stone, S.C., Rossetti, R.A.M., Alvarez, K.L.F., Carvalho, J.P., Margarido, P.F.R., Baracat, E.C., Tacla, M., Boccardo, E., Yokochi, K., Lorenzi, N.P., et al. (2019). Lactate secreted by cervical cancer cells modulates macrophage phenotype. J. Leukoc. Biol. *105*, 1041–1054. https://doi.org/10.1002/JLB.3A0718-274RR.